nature geoscience

ARTICLES

https://doi.org/10.1038/s41561-022-00920-7

Atmospheric CO_2 control of spontaneous millennial-scale ice age climate oscillations

Guido Vettoretti ✉, Peter Ditlevsen, Markus Jochum and Sune Olander Rasmussen

Last Glacial millennial-scale climate variability transitioned through distinct cold stadial and warm interstadial states. Here we use Earth system model simulations to demonstrate that nonlinear self-sustained climate oscillations appear spontaneously within a window of glacial-level atmospheric CO_2 concentrations (~190–225 parts per million). Outside this window, the system remains in either quasi-stable cold low CO_2 or warm high CO_2 states, with infrequent and abrupt random transitions driven by noise. In the oscillatory regime, the time between climate transitions is governed by temporal variations in the state of the ocean, atmosphere and sea ice, with CO_2 acting as a control on the relative rates of the internal forcing and feedback in the system. The Earth system model results map perfectly to a slow–fast dynamical systems model, where the fixed point of the system transitions into the oscillatory regime through a loss of stability at two critical tipping points, the window boundaries. The deterministic component of the oscillations is modified by a stochastic element associated with internal climate variability. Agreement between observations and the hierarchically disparate models suggests the existence of an internal stochastic climate oscillator, which tracks variations in atmospheric CO_2 level through the glacial, acting in concert with noise-induced transitions.

The Dansgaard–Oeschger (D–O) oscillation is a millennial-scale climate oscillation that alternated between cold stadial and warm interstadial states of up to 16 °C in amplitude at high northern latitudes during glacial periods[1]. In the Southern Hemisphere, the oscillation has a lower-amplitude counterpart with anti-phase characteristics[2–4]. Although several driving mechanisms have been suggested to explain D–O events, there now seems to be a consensus that jumps between different states of the Atlantic Meridional Overturning Circulation (AMOC) play an important role in the dynamics[5,6]. These abrupt changes in ocean circulation and, similarly, the North Atlantic sea-ice extent may involve noise-induced transitions between multiple equilibria in the climate system[7], forced either through stochastic[8–10] or coherence resonance[7,11,12]. Ocean oscillatory mechanisms may also arise because of advective or convective processes[13–15]. Internal free-running oscillations in a Stommel-type model[16] have also been proposed as a framework for explaining salinity oscillations under long-term forcing[17,18]. Similarly, the D–O oscillation exhibits behaviour in common with slow–fast dynamical systems[9,19–21]. Over the past few decades, simple models with 'deep-decoupling' oscillations[22,23] as well as more comprehensive coupled models[10,24–27] have demonstrated internal unforced climate oscillations in both modern and glacial climates. Other climate model simulations have invoked changes in Northern Hemisphere ice-sheet size[28] and secular CO_2 changes as triggers for the glacial climate transitions[29]. Furthermore, the concept of a window or sweetspot in past glacial climate conditions that favours abrupt transitions between warm and cold climate states has been proposed[22,27,29]; however, a satisfying mechanistic framework to explain these D–O events has remained absent.

A window of glacial millennial-scale climate variability

Marine Isotopic Stage 3 (MIS 3) is a period within the last ice age between approximately 60,000 and 28,000 years before present (Greenland Interstadial GI-17 to GI-3). MIS 3 atmospheric CO_2 concentrations declined steadily from ~230 parts per million by volume (ppm) until reaching Last Glacial Maximum (LGM) levels of ~190 ppm (Fig. 1a). The duration of warm interstadial and cold stadial periods changed throughout MIS 3, with long interstadial and short stadial periods in the beginning of this period, much debated regularity in the oscillations in the middle of this period[7,30], and long stadial and short interstadial periods near the LGM[31]. The glacial CO_2 record[32] and the temperature record in Antarctica[3] demonstrate that cold stadial periods were marked with massive iceberg discharge from Northern Hemisphere ice sheets (Heinrich events[33]), accompanied by strong temporary increases in CO_2 concentration of 10–20 ppm, which persisted past the end of each stadial. To quantify the connection between atmospheric CO_2 and the millennial-scale climate behaviour, we performed a set of eight 10,000-year-long equilibrated glacial simulations using a comprehensive climate model (CCSM4[34]), with different concentrations of MIS 3 atmospheric CO_2 in the range of 170–240 ppm (Extended Data Table 1 and Extended Data Fig. 1). Additionally, a glacial simulation with prescribed freshwater forcing of 0.05 Sv (1 Sverdrup $= 1 \times 10^6\ m^3\ s^{-1}$) for 500 years applied to the North Atlantic was run to simulate Heinrich events (iceberg melt). Two modern-day control experiments with original and modified ocean vertical mixing were used for model validation (Methods and Extended Data Fig. 2).

North Atlantic Deep Water (NADW) is formed in the Labrador, Irminger and Norwegian Seas, whereas Antarctic Bottom Water (AABW) is formed from regional variations in sea-ice brine rejection as well as ocean–ice shelf interactions mainly in the Ross and Weddell seas[35]. In a zonally averaged sense, these deep and bottom waters are components of an AABW cell that circulates in the opposite direction (anticlockwise) to an AMOC cell in the North Atlantic (clockwise) (Extended Data Fig. 3). Figure 2 presents six (of eight) CCSM4 simulations with different background levels of constant CO_2 concentration. The time series of AMOC maximum volume transport in the North Atlantic as well as the global zonal mean AABW maximum volume transport in the deep Southern Ocean are compared in Fig. 2a. Modelled Greenland (NGRIP) surface

Physics of Ice, Climate and Earth, Niels Bohr Institute, University of Copenhagen, Copenhagen, Denmark. ✉e-mail: gvettoretti@nbi.ku.dk

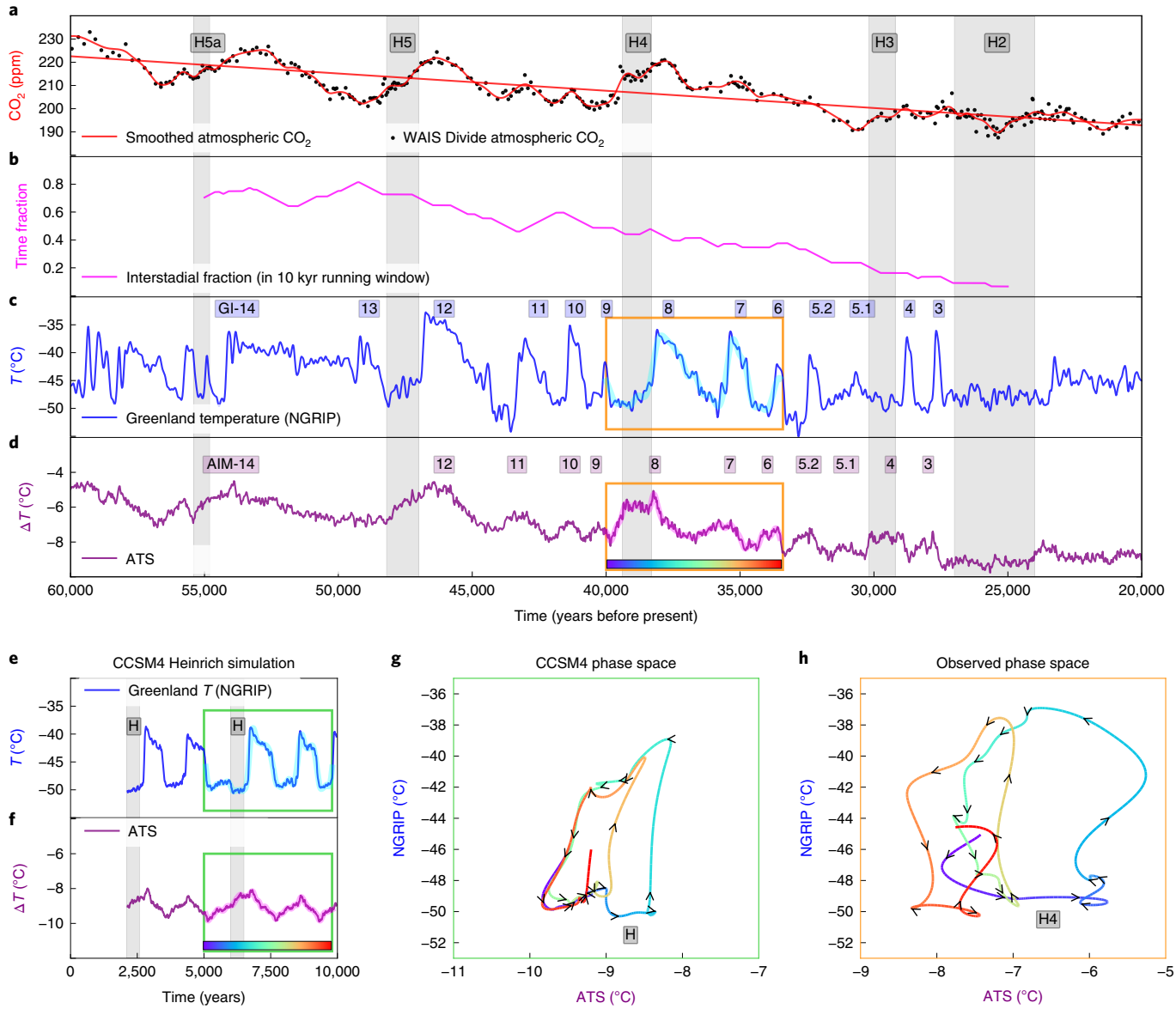

Fig. 1 | MIS 3 climate variability. a, Atmospheric CO_2 concentration (in ppm), showing a linear trend[32]. WAIS, West Antarctic Ice Sheet. **b**, Time fraction spent in interstadials[36]. **c**, NGRIP Greenland temperature (T) reconstruction based on $\delta^{15}N$ and $\delta^{18}O$ (ref. [3]). NGRIP, North Greenland Ice Core Project. **d**, ATS based on $\delta^{18}O$ and δD records from six Antarctic ice cores[3]. **e**, Temperature at NGRIP in CCSM4 ($CO_2 = 210$ ppm). **f**, As in **e**, but for the CCSM4-derived ATS (ΔT). **g**, Model ATS versus model NGRIP temperature from the green boxes in **e** and **f**. **h**, Observed ATS versus observed NGRIP temperature from the orange boxes in **c** and **d**. Colour bars in **d** and **f** measure time in **g** and **h** (black arrowheads indicate the direction of time with units of 250 and 300 years for model and observations, respectively). The phase space time series have been low-pass-filtered (transparent cyan and fuchsia in **c**–**f**; Supplementary Information). ATS temperatures are anomalies from modern (ΔT). Heinrich events (H) are represented by grey vertical bars, Greenland Interstadials (GI) by blue squares and their associated Antarctica Isotope Maxima (AIM) by purple squares.

temperature (Fig. 1e) is in phase with the modelled AMOC transport (Fig. 2e). The modelled Antarctic Temperature Stack (ATS; Fig. 1f) is, however, 180° out of phase with the modelled AABW transport (Fig. 2e). Warming in Greenland is associated with strengthening NADW production, whereas warming in Antarctica is associated with weakening AABW production. The simulations demonstrate that, at high CO_2 levels, warm Greenland interstadials (characterized by stronger AMOC) are longer than cold Greenland stadial periods (characterized by weaker AMOC). As the CO_2 level is reduced, the duration of the stadial part of the D–O oscillation steadily increases, while the interstadial part becomes shorter. In an intermediate range of CO_2 concentrations (200–225 ppm), the model exhibits quasi-periodic oscillations between the stadial and interstadial states. The oscillations are not quite regular due to internal climate variability (noise), but the approximate period and shape are close to observations from Greenland (NGRIP) ice-core temperature proxy records[36] as well as marine-based AMOC proxy records of lateral deep water-mass export away from the North Atlantic[37]. At both extreme levels of high and low CO_2, the model oscillations are absent.

The strength of the NADW production (or AMOC maximum) is often compared against some imposed freshwater forcing on the surface of the high-latitude North Atlantic ocean to study hysteresis in an ocean model[38]. Here we use AABW as a representation of the slowly varying integrated buoyancy gain and loss rates around Antarctica (the forcing)[39], and the AMOC represents the

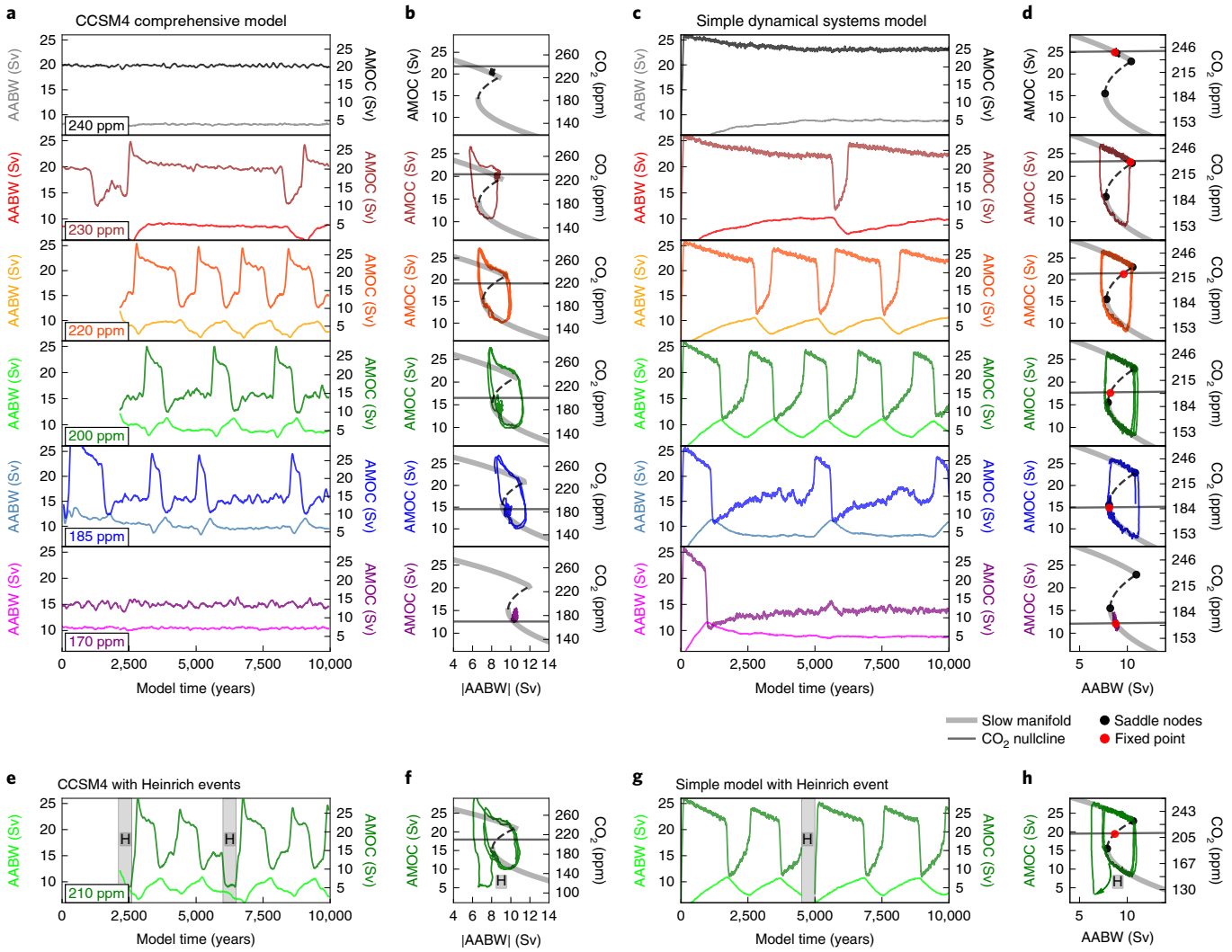

Fig. 2 | Comprehensive and simple model D–O simulations. a, D–O oscillations in CCSM4 at different atmospheric CO_2 concentration. Time series of AABW (left inverted *y* axis) and AMOC (right) strength (larger negative AABW values equal increasing AABW strength). **b**, Ocean circulation phase space: AMOC versus the magnitude of AABW. **c**, Simple dynamical systems model at different levels of atmospheric CO_2, with stochastic forcing applied. **d**, Simple model phase space diagram. **e**, Heinrich events simulated with freshwater forcing added to the North Atlantic in CCSM4 during two D–O stadials. **f**, CCSM4 Heinrich ocean phase space. **g**, Heinrich-like forcing applied at year 4,500 in the simple model (the system evolves from a new initial condition). **h**, Simple model Heinrich phase space (green arrow marks the freshwater forcing response). CCSM4 model (simple model) phase space diagrams use years 5,000 (3,000) to 10,000 of the corresponding time series. The CCSM4 data are smoothed with a 100-year running mean, and the CCSM4 phase space has a 100-year time lag removed between the AABW and AMOC. Shown in each phase space diagram are the slow manifold (light grey), the linear nullcline (dark grey) and the separatrix (dashed), with the right axis illustrating the CO_2 nullcline level as well as the system fixed point (red dot) and critical points (black dots).

fast-timescale dynamics reacting to the slowly varying processes within the climate system (mainly in the Atlantic). The AABW and AMOC time series (Fig. 2a) are used to construct a slow–fast representation of the global D–O oscillation, which results in an effective two-dimensional (2D) phase space representation of the comprehensive model D–O cycle (Fig. 2b). A comparison can be made between the mirrored orientation seen in the comprehensive model NGRIP-ATS and AMOC-AABW phase space portraits (compare Figs. 1g and 2f). On shorter timescales, buoyancy loss in high-latitude northern deep-water and southern bottom-water formation sites must be compensated by buoyancy gain in either the interior low-latitude ocean through mixing across density surfaces or through direct surface buoyancy forcing in the ventilated thermocline at higher latitudes (for example, along the sea-ice edge in the Southern Ocean)[4,27,39–43]. On the millennial timescale, the glacial global ocean in the comprehensive model gains buoyancy during a cold stadial period, mainly by increasing ocean heat content in the Southern Hemisphere oceans and under North Atlantic sea ice. This excess heat is then re-emitted to space during the ensuing interstadial period[3,25]. Increases in buoyancy flux into the ocean during stadials stratify the global ocean. The phase-space representation therefore implies that the AMOC has a fast response to slow changes in global average stratification. The slow-timescale evolution of the closure of the overturning circulation is therefore implicitly represented in the phase-space portraits of the northern and southern overturning circulation.

The stochastic climate oscillator

The conceptual model presented here is based on a Stommel[16] density-driven box model framework in a modified context[17,18] and

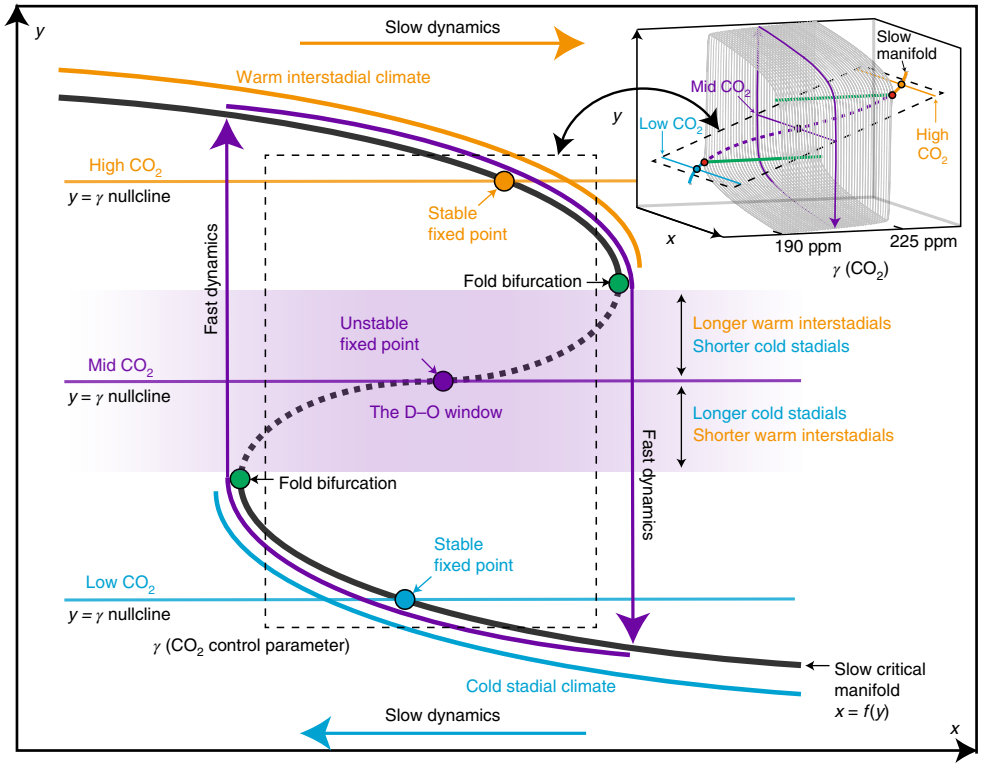

Fig. 3 | The double-fold bifurcation. Schematic of the low-dimensional structure of glacial millennial-scale climate variability. The dynamical system (equation (1)) has a slow critical manifold structure on which the slow dynamics evolve. The upper and lower branches (black curved solid lines) of the slow manifold represent two equilibrium branches of the AMOC (y), and the black curved dashed line indicates the separatrix between the two (inset purple curved dashed line). The slow manifold and the $y=\gamma$ nullcline are invariant manifolds determined by the time-invariant properties of the system. The fixed point of the system is determined by the intersection of these two invariant manifolds and results in a climate state that is stable (non-oscillatory; blue and orange circles) or unstable (oscillatory; purple circle). The stability of the climate state is therefore controlled by the level of atmospheric CO_2 concentration. As the CO_2 control parameter (γ) evolves into a mid-range of CO_2 concentration (~190–225 ppm) from either high or low CO_2 concentration, the system undergoes a Hopf-bifurcation (inset red circles) where oscillations appear (the purple D–O window). The relative duration of interstadials and stadials is determined by the proximity of the unstable fixed point to either fold bifurcation (green circle, inset green line). For CO_2 concentration below ~190 ppm or above 225 ppm, the y-nullcline crosses the lower or upper branch of the slow manifold, where the climate is in either a stable fixed cold or warm state, respectively. The dashed square represents a plane formed by a range of $y=\gamma$ nullclines that intersect the slow manifold at different levels of CO_2 concentration (inset).

is used as a template to explain some of the behaviour observed in our comprehensive climate-model simulations (Supplementary Information). The simple model combines fast Atlantic meridional temperature and salinity variations as well as the slow evolution of the global freshwater and heat forcing in a simplified buoyancy framework. The AMOC (y) and AABW (x) represent the main variables of an effective slow–fast excitable system controlled by the atmospheric CO_2 concentrations (γ). The time-dependent (t) physical behaviour of such a system can be illustrated by the following set of equations (Fig. 3):

$$\begin{aligned} \mathrm{d}y &= (f(y) - x)\mathrm{d}t/\tau_y + \sigma_y \mathrm{d}W_t \\ \mathrm{d}x &= (y - \gamma)\mathrm{d}t/\tau_x + \sigma_x \mathrm{d}W_t \end{aligned} \quad (1)$$

where $\tau_x \gg \tau_y$ are the slow and fast timescales of the system, respectively. The small parameter $\epsilon = \tau_y/\tau_x$ allows for the separation of all motions into only fast changes in y and slow ones in $x \approx f(y)$, the slow critical manifold. Here we model the nonlinear evolution of the system as a non-smooth Stommel-type system with $f(y) = -c\,y\,|a + b\,c\,y| + d$, where ($a$, b, c, d) are parameters (Methods and Extended Data Fig. 4). This system is characterized by a double-fold bifurcation structure (Fig. 3) with either a stable non-oscillatory or unstable oscillatory fixed point dependent on the value of the control parameter (γ). Internal climate variability is represented by an additional diffusion term ($\sigma \mathrm{d}W_t$) with variance (σ). The model presented in equation (1) is given as the simplest representation of our slow–fast system. This model has been configured and enhanced (Methods and Supplementary Information) with a set of adjustable physically based parameters (obtained from the comprehensive climate model) to reproduce the complex model behaviour (Fig. 2b,d). We estimate the slow e-folding timescale of the recharge/discharge heat oscillator[44] below the sea-ice lid in the North Atlantic to be ~150 years, which influences the period of the oscillation. The fast timescale corresponds to the advection timescale of the AMOC using the volume of the North Atlantic box in the simple model (~10 years). The salt-advection feedback in the simple model has been configured based on linear relationships derived from the meridional density gradient and salt convergence/divergence in the Atlantic sector obtained from the comprehensive model diagnostics (Supplementary Information). This dynamical system (equation (1)) includes nonlinear damping associated with the nonlinear terms in the first equation, and ones that shape the slow manifold. At intermediate AMOC strength, the system exhibits negative damping, during which signals are amplified, and at extrema in AMOC strength, the system exhibits strong positive

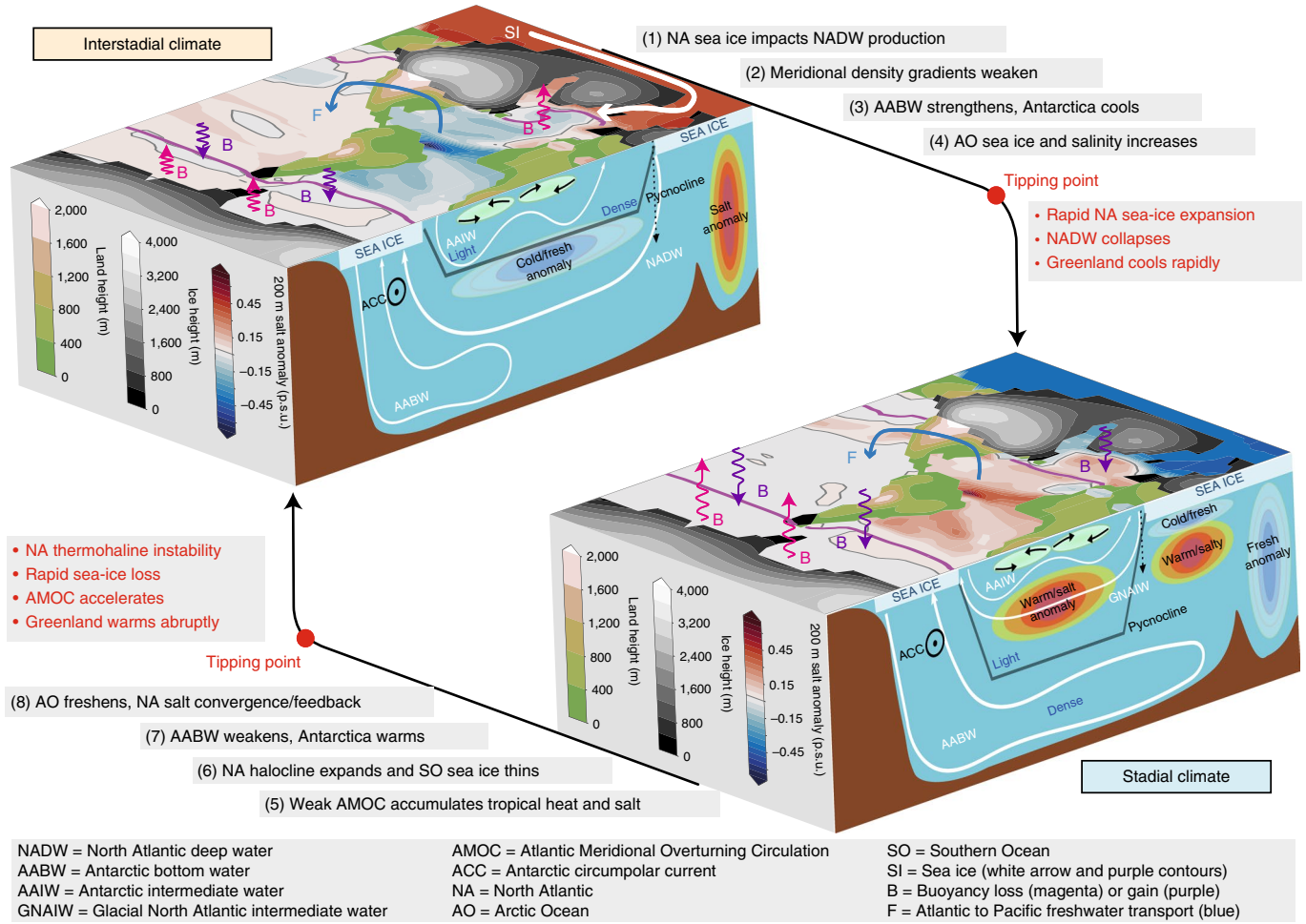

Fig. 4 | Transitions between interstadial and stadial climate. Atmospheric CO_2 controls the rate of approach to the climate tipping point. Low CO_2 results in longer stadial duration, faster North Atlantic sea-ice growth, reduced Atlantic-to-Pacific vapour transport, stronger atmospheric meridional temperature gradients and stronger (weaker) AABW (NADW) formation. High CO_2 results in shorter stadial duration, enhanced convective available potential energy below the North Atlantic halocline, accelerated North Atlantic sea-ice loss, enhanced Atlantic-to-Pacific vapour transport, enhanced salt feedback and weaker AABW formation. (1–4) Old Arctic sea ice is exported to the North Atlantic, sea-ice melt reduces high-latitude convection, ice-albedo feedback favours sea-ice growth, and Greenland and Antarctica cool. The interstadial-to-stadial tipping point occurs with rapid North Atlantic sea-ice expansion and a collapse of NADW production. (5–8) North Atlantic sea-ice halocline expands southward, sub-sea-ice temperature and salinity increase, meridional density gradients weaken and vertical stratification increases. Equatorial Atlantic Ocean heat anomalies are advected and diffused to the North Atlantic and Southern Ocean. During the cool North Atlantic stadial, Antarctica warms and Southern Ocean sea ice thins. Salt convergence increases in the North Atlantic, salt advection feedback amplifies NADW fluctuations, and late-stadial reductions in AABW formation allow the volume of NADW to increase. Late-stadial high-latitude North Atlantic vertical stratification undergoes thermohaline instability and destabilizes the Irminger and Nordic Seas, tipping the system from stadial to interstadial and resulting in rapid North Atlantic sea-ice loss. Greenland then warms abruptly, followed by gradual Antarctic and Greenland cooling. The D–O cycle then repeats. p.s.u., practical salinity units.

damping that restores the signal back to an intermediate amplitude. At low CO_2 levels near the lower fold-bifurcation, the addition of noise to this stable simple model simulation (Fig. 2c) produces short and relatively infrequent interstadials, as is observed in the comprehensive model simulation.

The glacial climate response to CO_2 and Heinrich events

The physical impacts of atmospheric CO_2 in the complex climate model are numerous (Fig. 4). The CO_2 forcing and resulting feedbacks within the system determine the rates at which critical mechanisms in the D–O cycle operate (Fig. 3). We find increases in the stadial salinity of the Atlantic and a stadial freshening of the Pacific in simulations, with higher CO_2 levels compared with the ensemble mean (Extended Data Fig. 5). Larger stadial versus interstadial low-latitude salinity in individual simulations is mainly due to reductions in northward salt transport during the stadial. Therefore, increases in the background CO_2 level increase stadial low-latitude salinity relative to the ensemble through increased Atlantic to Pacific atmospheric vapour transport. This model exhibits self-sustained oscillation, regardless of the CO_2 level (albeit within the D–O window), in contrast to previous studies that used secular CO_2 changes to trigger individual transitions[29]. Here, the CO_2 control parameter impacts the salinity convergence in the North Atlantic, which affects the rate of salt advection feedback in each simulation, a critical component in terminating the stadial climate state[45]. The CO_2 control parameter also impacts ocean heat content (Extended Data Fig. 6) and Arctic and North Atlantic sea ice (Extended Data Fig. 7), moderating stadial and interstadial duration. The interstadial is terminated by the advection of sea ice from an Arctic reservoir into the North Atlantic regions of NADW formation, and the

stadial is terminated by the release of ocean heat content in the same region[46]. The CO_2 concentration impacts the amount of ocean heat content and the mean sea-ice volume in these critical high-latitude regions. In particular, the same window of CO_2-dependent tipping point behaviour is observed in the Arctic sea-ice volume (Extended Data Fig. 7). At low and high CO_2, the system maintains constant levels of sea-ice volume, whereas, at intermediate CO_2 levels, the sea ice fluctuates with a consistent level of large variability between stadial and interstadial but with secular changes in the mean.

Phase-space trajectories (Fig. 2) show that D–O warming events in the simple model lack the physical behaviour to overshoot the upper slow manifold (as is observed in the complex model). In the complex model, the stadial ends with convective thermohaline instability under the sea-ice-covered North Atlantic sub-polar gyre, which acts as a tipping point[47]. This instability leads to the initial sharp rise in temperatures observed at NGRIP during D–O warming events. The overshoot (abrupt warming versus cooling asymmetry) seen in the comprehensive model is a fairly well-resolved feature in ice-core records[36]. The additional comprehensive model Heinrich simulation in which we impose freshwater forcing to the North Atlantic during two stadial periods (Fig. 2e) has a larger AMOC and Northern Hemisphere temperature overshoot (Fig. 1e) after the Heinrich stadial ends. However, this rapid AMOC increase above regular interstadial levels is consistent with observations only for a select few Heinrich stadial periods (for example, H4 and H5[37]). The simple model implies that the climate system response to Heinrich events corresponds with a perturbation to a climate trajectory where the system must transition over a longer distance in phase space to reach the upper portion of the slow climate manifold and therefore results in a stronger AMOC recovery (Fig. 2h). The lengthening of the stadial period is associated with additional Heinrich-event-related buoyancy input to the North Atlantic; however, the low number of observed Heinrich events makes it difficult to attribute much statistical significance to the lengthening. MIS 3 ice-core records from Greenland, as well as marine-based records, also show that D–O oscillations occur in the absence of Heinrich events throughout the last glacial cycle[36,37]. A previous study[25] invoked a 'kicked' salt oscillator hypothesis (or a pseudo-Heinrich type behaviour) to provide a kick that induces a D–O salt oscillation. The oscillations should then dissipate after the initial perturbation, but it was hypothesized that the system had a high quality (Q) factor to explain the constant-amplitude periodicity observed. The spontaneous D–O oscillations simulated here do not require Heinrich events to operate.

Towards a comprehensive theory for D–O events

A comprehensive theory for the D–O oscillation will require an understanding of how various other components of the Earth system impact and modify the nonlinear system described here. Glacial CO_2 levels result from ocean and land biogeochemical processes responding to internal and external forcing and will therefore modulate the oscillations. Heinrich events (through the associated CO_2 rise) may be an integral part of the internal climate oscillator, and not solely a component that affects stadial duration. Recent reconstructions of MIS 3 land ice-sheet size[48] demonstrate median ice volumes between the LGM and modern size. This implies a range of relative sea level where the Bering Strait may have been open or closed, impacting freshwater transport between the Pacific and Arctic oceans. Glacial ice sheets also impact the Northern Hemisphere jet stream and North Atlantic sub-polar gyre dynamics. A more zonal, less variable LGM North Atlantic jet stream becomes more variable and fluctuates over a larger range of latitudes as the ice sheets are changed towards a more modern configuration[6]. MIS 3 ice sheets should provide a setting for a sensitive interplay between the sea-ice edge in the sub-polar gyre region during glacial periods[10,49]. Nonlinear sub-polar gyre dynamics[50] may indeed play a crucial role in D–O event formation. Climate model studies need to place the multi-decadal to centennial variability and hysteresis observed in models of the North Atlantic into the context of noise-induced glacial climate transitions either through wind-strength variations or buoyancy-driven anomalies[49]. Therefore, coherent resonant excitation[7] of D–O events may arise from purely noise-driven processes that exist internally in the climate system[6,49]. Stochastic resonant excitation[8] of D–O events may be associated with some low-amplitude signal originating from irregular multi-decadal to multi-centennial variations in solar or volcanic forcing within the climate system[51]. Spontaneous millennial-scale oscillations can also occur in modern climate simulations under different atmospheric CO_2 concentration as well as changes in the Earth's orbital configuration[26,27]. The Earth's orbital obliquity and eccentricity-precession-induced boreal summer seasonality will impact glacial North Atlantic sea-ice cover and therefore modulate the D–O oscillation[26]. The D–O oscillation may also be sensitive to increased tidal forcing and deep energetic mixing in the ocean[52] resulting from changes in continental ice-sheet size. Therefore, contingent on the uncertainty associated with these other mechanisms described here, the D–O window and the low-order dynamical structure of the glacial climate system may evolve or the hysteretic structure may even collapse under evolving glacial forcing and boundary conditions. Finally, different Earth system model biases will need to be investigated to constrain the range of atmospheric CO_2 bounding this D–O sweetspot.

Online content

Any methods, additional references, Nature Research reporting summaries, source data, extended data, supplementary information, acknowledgements, peer review information; details of author contributions and competing interests; and statements of data and code availability are available at https://doi.org/10.1038/s41561-022-00920-7.

Received: 8 March 2021; Accepted: 25 February 2022;
Published online: 07 April 2022

References

1. Dansgaard, W. et al. Evidence for general instability of past climate from a 250-kyr ice-core record. *Nature* **364**, 218–220 (1993).
2. Stocker, T. F. & Johnsen, S. J. A minimum thermodynamic model for the bipolar seesaw. *Paleoceanogr. Paleoclimatol.* **18**, 1087 (2003).
3. Pedro, J. B. et al. Beyond the bipolar seesaw: toward a process understanding of interhemispheric coupling. *Quat. Sci. Rev.* **192**, 27–46 (2018).
4. Thompson, A. F., Hines, S. K. & Adkins, J. F. A Southern Ocean mechanism for the interhemispheric coupling and phasing of the bipolar seesaw. *J. Clim.* **32**, 4347–4365 (2019).
5. Dijkstra, H. A. *Nonlinear Climate Dynamics* (Cambridge Univ. Press, 2013).
6. Li, C. & Born, A. Coupled atmosphere–ice–ocean dynamics in Dansgaard–Oeschger events. *Quat. Sci. Rev.* **203**, 1–20 (2019).
7. Ditlevsen, P. D., Kristensen, M. S. & Andersen, K. K. The recurrence time of Dansgaard–Oeschger events and limits on the possible periodic component. *J. Clim.* **18**, 2594–2603 (2005).
8. Véez-Belchí, P., Alvarez, A., Colet, P., Tintoré, J. & Haney, R. L. Stochastic resonance in the thermohaline circulation. *Geophys. Res. Lett.* **28**, 2053–2056 (2001).
9. Ganopolski, A. & Rahmstorf, S. Abrupt glacial climate changes due to stochastic resonance. *Phys. Rev. Lett.* **88**, 038501 (2002).
10. Kleppin, H., Jochum, M., Otto-Bliesner, B., Shields, C. A. & Yeager, S. Stochastic atmospheric forcing as a cause of Greenland climate transitions. *J. Clim.* **28**, 7741–7763 (2015).
11. Cessi, P. A simple box model of stochastically forced thermohaline flow. *J. Phys. Ocean.* **24**, 1911–1920 (1994).
12. Timmermann, A., Gildor, H., Schulz, M. & Tziperman, E. Coherent resonant millennial-scale climate oscillations triggered by massive meltwater pulses. *J. Clim.* **16**, 2569–2585 (2003).
13. Winton, M. & Sarachik, E. Thermohaline oscillations induced by strong steady salinity forcing of ocean general circulation models. *J. Phys. Ocean.* **23**, 1389–1410 (1993).
14. Sévellec, F., Huck, T. & Ben Jelloul, M. On the mechanism of centennial thermohaline oscillations. *J. Mar. Res.* **64**, 355–392 (2006).

15. Colin de Verdière, A. A simple model of millennial oscillations of the thermohaline circulation. *J. Phys. Ocean.* **37**, 1142–1155 (2007).
16. Stommel, H. Thermohaline convection with two stable regimes of flow. *Tellus* **13**, 224–230 (1961).
17. Berglund, N. & Gentz, B. *Noise-Induced Phenomena in Slow–Fast Dynamical Systems: A Sample-Paths Approach* (Springer, 2006).
18. Roberts, A. & Saha, R. Relaxation oscillations in an idealized ocean circulation model. *Clim. Dyn.* **48**, 2123–2134 (2017).
19. Rial, J. & Saha, R. Modeling abrupt climate change as the interaction between sea ice extent and mean ocean temperature under orbital insolation forcing. *Agu. Geophys. Mono.* **193**, 57–74 (2011).
20. Crucifix, M. Oscillators and relaxation phenomena in Pleistocene climate theory. *Philos. Trans. R. Soc. A* **370**, 1140–1165 (2012).
21. Kwasniok, F. Analysis and modelling of glacial climate transitions using simple dynamical systems. *Philos. Trans. R. Soc. A* **371**, 20110472 (2013).
22. Sima, A., Paul, A. & Schulz, M. The Younger Dryas—an intrinsic feature of late Pleistocene climate change at millennial timescales. *Earth Planet. Sci. Lett.* **222**, 741–750 (2004).
23. Olsen, S. M., Shaffer, G. & Bjerrum, C. J. Ocean oxygen isotope constraints on mechanisms for millennial-scale climate variability. *Paleoceanogr. Paleoclimatol.* **20**, PA1014 (2005).
24. Arzel, O., England, M. H., de Verdière, A. C. & Huck, T. Abrupt millennial variability and interdecadal-interstadial oscillations in a global coupled model: sensitivity to the background climate state. *Clim. Dyn.* **39**, 259–275 (2012).
25. Peltier, W. R. & Vettoretti, G. Dansgaard-Oeschger oscillations predicted in a comprehensive model of glacial climate: a 'kicked' salt oscillator in the Atlantic. *Geophys. Res. Lett.* **41**, 7306–7313 (2014).
26. Brown, N. & Galbraith, E. D. Hosed vs. unhosed: interruptions of the Atlantic Meridional Overturning Circulation in a global coupled model, with and without freshwater forcing. *Clim. Past* **12**, 1663–1679 (2016).
27. Klockmann, M., Mikolajewicz, U. & Marotzke, J. Two AMOC states in response to decreasing greenhouse gas concentrations in the coupled climate model MPI-ESM. *J. Clim.* **31**, 7969–7984 (2018).
28. Zhang, X., Lohmann, G., Knorr, G. & Purcell, C. Abrupt glacial climate shifts controlled by ice sheet changes. *Nature* **512**, 290–294 (2014).
29. Zhang, X., Knorr, G., Lohmann, G. & Barker, S. Abrupt North Atlantic circulation changes in response to gradual CO_2 forcing in a glacial climate state. *Nat. Geosci.* **10**, 518–523 (2017).
30. Schulz, M., Berger, W. H., Sarnthein, M. & Grootes, P. M. Amplitude variations of 1,470-year climate oscillations during the last 100,000 years linked to fluctuations of continental ice mass. *Geophys. Res. Lett.* **26**, 3385–3388 (1999).
31. Lohmann, J. & Ditlevsen, P. D. Random and externally controlled occurrences of Dansgaard–Oeschger events. *Clim. Past* **14**, 609–617 (2018).
32. Bauska, T. K., Marcott, S. A. & Brook, E. J. Abrupt changes in the global carbon cycle during the last glacial period. *Nat. Geosci.* **14**, 91–96 (2021).
33. Heinrich, H. Origin and consequences of cyclic ice rafting in the northeast Atlantic Ocean during the past 130,000 years. *Quat. Res.* **29**, 142–152 (1988).
34. Gent, P. R. et al. The Community Climate System Model version 4. *J. Clim.* **24**, 4973–4991 (2011).
35. Ohshima, K. I. et al. Antarctic bottom water production by intense sea-ice formation in the Cape Darnley polynya. *Nat. Geosci.* **6**, 235–240 (2013).
36. Rasmussen, S. O. et al. A stratigraphic framework for abrupt climatic changes during the last glacial period based on three synchronized Greenland ice-core records: refining and extending the INTIMATE event stratigraphy. *Quat. Sci. Rev.* **106**, 14–28 (2014).
37. Henry, L. G. et al. North Atlantic Ocean circulation and abrupt climate change during the last glaciation. *Science* **353**, 470–474 (2016).
38. Rahmstorf, S. On the freshwater forcing and transport of the Atlantic thermohaline circulation. *Clim. Dyn.* **12**, 799–811 (1996).
39. Jansen, M. F. & Nadeau, L.-P. A toy model for the response of the residual overturning circulation to surface warming. *J. Phys. Ocean.* **49**, 1249–1268 (2019).
40. Lumpkin, R. & Speer, K. Global ocean meridional overturning. *J. Phys. Ocean.* **37**, 2550–2562 (2007).
41. Nikurashin, M. & Vallis, G. A theory of the interhemispheric meridional overturning circulation and associated stratification. *J. Phys. Ocean.* **42**, 1652–1667 (2012).
42. Marshall, J. & Speer, K. Closure of the meridional overturning circulation through Southern Ocean upwelling. *Nat. Geosci.* **5**, 171–180 (2012).
43. Sun, S., Eisenman, I. & Stewart, A. L. Does Southern Ocean surface forcing shape the global ocean overturning circulation? *Geophys. Res. Lett.* **45**, 2413–2423 (2018).
44. Boers, N., Ghil, M. & Rousseau, D.-D. Ocean circulation, ice shelf, and sea ice interactions explain Dansgaard–Oeschger cycles. *Proc. Natl Acad. Sci. USA* **115**, E11005–E11014 (2018).
45. Drijfhout, S. S., Marshall, D. P. & Dijkstra, H. A. Ocean circulation and climate: a 21st century perspective. *Int. Geophys.* **103**, 257–282 (2013).
46. Vettoretti, G. & Peltier, W. R. Fast physics and slow physics in the nonlinear Dansgaard–Oeschger relaxation oscillation. *J. Clim.* **31**, 3423–3449 (2018).
47. Vettoretti, G. & Peltier, W. R. Thermohaline instability and the formation of glacial North Atlantic super polynyas at the onset of Dansgaard–Oeschger warming events. *Geophys. Res. Lett.* **43**, 5336–5344 (2016).
48. Gowan, E. J. et al. A new global ice sheet reconstruction for the past 80,000 years. *Nat. Commun.* **12**, 1199 (2021).
49. Klockmann, M., Mikolajewicz, U., Kleppin, H. & Marotzke, J. Coupling of the subpolar gyre and the overturning circulation during abrupt glacial climate transitions. *Geophys. Res. Lett.* **47**, e2020GL090361 (2020).
50. Born, A. & Stocker, T. F. Two stable equilibria of the Atlantic subpolar gyre. *J. Phys. Ocean.* **44**, 246–264 (2014).
51. Svensson, A. et al. Bipolar volcanic synchronization of abrupt climate change in Greenland and Antarctic ice cores during the last glacial period. *Clim. Past* **16**, 1565–1580 (2020).
52. Schmittner, A., Green, J. A. M. & Wilmes, S.-B. Glacial ocean overturning intensified by tidal mixing in a global circulation model. *Geophys. Res. Lett.* **42**, 4014–4022 (2015).

Methods

Comprehensive model simulations. The D–O oscillations modelled in this study were simulated using the low-resolution version of the Community Climate System Model Version 4 (CCSM4[54]), a model of ~3×3° that employs CAM4[53] and POP2[54] as the atmosphere and ocean components, respectively. The model is part of the Community Earth System Model release version 1 (CESM1-CAM4). The land surface is represented by CLM4[55] and the sea-ice dynamics by CICE4[56]. The glacial climate experiments use LGM ice-age boundary conditions from the ICE-6G series of model palaeotopography, bathymetry and land-ice cover characteristic of LGM[57,58]. MIS 3 ice sheets are thought to have evolved substantially between 52 ka BP and 40 ka BP[59,60] and are expected to influence the dynamics of the D–O cycle[61]; however, the ice sheets here are fixed with the purpose of investigating perturbations of the D–O cycle to Heinrich (H) events and atmospheric CO_2 forcing. The model and methodology for producing the ice-sheet boundary conditions have been discussed in detail previously[62]. The transition depth of the ocean vertical mixing profile is set to 2,500 m in a Bryan and Lewis type of formulation[63]. The new glacial climate simulations are consistent with the original D–O simulations from refs. [25,46], but have a D–O period that is longer and more accurate with regard to observations. The experiments with this model include freshwater perturbations[64] applied to the North Atlantic, as well the use of different constant levels of observed MIS 3 CO_2 concentration in the experiments.

A series of modern and glacial climate simulations run with CCSM4 are summarized in Extended Data Table 1. Two long pre-industrial (PI) climate simulations were run to investigate the influence of ocean-mixing changes made in the glacial climate simulations on the PI climate. The series of glacial simulations span a range of CO_2 levels from 170 ppm to 240 ppm, and a subset of the glacial climate simulations were branched off an initial simulation that was spun up for ~2,100 years with a CO_2 concentration of 185 ppm. Some of the runs with low or high CO_2 or those that were near a saddle node bifurcation point were run for a longer period. The set of simulations branched from this initial glacial (CO_2 = 185 ppm) run required another 3,000 years of simulation to reach equilibrium, where a statistically stationary stable internal D–O oscillatory pattern emerged. Three of the simulations (170 ppm, 230 ppm and 240 ppm) were run for ~13,000 years, but only the last 10,000 years are shown in the plots. An additional simulation was run with a Heinrich event (H event)-like pulse of freshwater of 0.05 Sv for 500 years in two different (regular D–O) stadial periods in the simulation with a CO_2 level of 210 ppm (years 2,100–2,600 and 6,000–6,500). The square pulse of freshwater was applied to the North Atlantic from 50° N to 70° N, but the freshwater was allowed to remain in the ocean and reduce the global average salinity. Each pulse corresponds to an equivalent relative sea level increase of ~1.8 m (but the topography/bathymetry was not modified).

Each of the individual glacial climate simulations with different levels of atmospheric CO_2 produces D–O oscillations of varying period, and some of the initial variations in the simulation are probably due to disequilibrium of the mean ocean climate state. Some of the simulations were branched from the simulation with 185 ppm at the year 2,100, so the higher CO_2 simulations need time to equilibrate to a warmer climate. The global mean temperature, salinity, density and ideal age (Extended Data Fig. 1) in the glacial climate simulations have significant trends over the 10,000-year lengths of the runs. Notably, in terms of the mean temperature, it appears to take at least 3,000 years before temperatures start to equilibrate (Extended Data Fig. 1a). The mean salinity has the same small decreasing trend that is also seen in the PI simulations (Extended Data Figs. 1b and 2d), but salinity is almost conserved. The variations in temperature affect the density, but the density variations seem to take more time to reach equilibrium (Extended Data Fig. 1c). The ideal age, an approximate diagnostic of ventilation ages, does not appear to reach equilibrium until ~8,000 years (Extended Data Fig. 1d). Generally, the regularity of the D–O oscillations in this mid-range of CO_2 levels appears to stabilize in the second half of each glacial simulation.

PI climate validation. The MIS 3 glacial climate simulations that produce spontaneous internal D–O oscillations have a modified ocean mixing parameterization[63], as described above. POP2 implements a tidal mixing parameterization that is used to capture the influence of diabatic mixing due to internal wave breaking generated by the interaction of the barotropic tide and ocean bathymetric features (for example, mid-ocean ridges)[65]. The re-introduction of the more simple constant vertical diffusivity[63] profile in CCSM4, as well as the removal of an overflow parameterization[66], was implemented because the exact bathymetry and tidal energy field during the glacial is unknown (relative sea level was much lower than the modern level). The overflow parameterization would also not be compatible with glacial ocean bathymetry, and therefore the simplest choice is to remove both modern parameterizations. The modification of the ocean model, which will be used for our long simulations, therefore requires some modern climate validation. We have thus run the original low-resolution simulation[67] for 3,000 years, but with the ocean mixing parameterizations turned off, and instead used a simple vertical mixing profile[63] with a transition depth at 2,500 m. The main problems with the original version of the model were slightly excessive sea ice in the high northern latitudes and cold fresh conditions at the ocean surface[67]. These problems still persist in the modified version of the model. The modern time evolution of the global profiles of temperature and salinity in the ocean are shown in Extended Data Fig. 2. There is slight excessive cooling at the surface and slight excessive warming around the pycnocline depth, but the trends remain very stable after 1,000 years.

In each of the PI and glacial climate simulations, the diagnosed AMOC maximum is calculated from the region below 500 m and between 25° N and 40° N (Extended Data Fig. 3). AABW is also used as a diagnostic, but because this circulation is in the opposite direction of the AMOC streamfunction, the maximum strength is determined from the largest negative value in the Southern Ocean between 80° S and 0°, below 3,000 m. The AABW maximum strength is inverse to the strength of the AMOC maximum (the NADW formation rate in the North Atlantic). The temperatures over Greenland and Antarctica in the complex model glacial simulations are correlated with AMOC and AABW, respectively, except that temperatures in Antarctica are anti-phase to the strength of the AABW formation rate. The main changes in the PI AMOC structure with changes in ocean vertical mixing are a shoaling of the NADW level by ~1,000 m in the North Atlantic, which is a problem with the modified model, and one of the main reasons why the new parameterizations were implemented into CCSM4 (the overflow parameterization[66] is especially important in ameliorating this problem). However, deep water formation in the Southern Ocean was found to deteriorate slightly with the implementation of the overflow parameterization. The rate of Antarctic bottom water in the modified model appears to be more in line with observations[68] and may be an important component in simulating D–O oscillations, or at least bipolar aspects of the D–O oscillation. The meridional overturning circulation in the modified PI model has a circulation regime that is more adiabatic[69], rather than a diffusive regime as in the original version of the model. The AMOC is weaker in our modified version, but the AABW is stronger and therefore more balanced (Extended Data Fig. 3b). Atlantic bottom water formation is stronger, while Pacific bottom water formation is weaker in our modified version (not shown). The Indian sector has more minor changes and is not shown. The stadial glacial NADW cell is deeper than modern in the glacial interstadial period (Extended Data Fig. 3d), but it is shallower in the glacial stadial period compared with the modern (Extended Data Fig. 3c).

The simple model and the slow manifold structure. The conceptual model presented here is based on a Stommel[16] density driven box model framework (Supplementary Information). The deterministic component of the simple system used to model the physical behaviour has the following representation:

$$\begin{aligned} \frac{dy}{dt} &= (f(y) - x)/\tau_y \\ \frac{dx}{dt} &= (y - \gamma)/\tau_x \end{aligned} \tag{2}$$

where $\tau_x \gg \tau_y$ are the slow and fast timescales of the system, respectively. The time-invariant ($\frac{d}{dt} = 0$) properties of the system constrain the slow motions (the slow manifold, $x = f(y)$) of the system, as well as determining the fixed point of the system (intersection of the slow manifold with $y = \gamma$) governed by the control parameter (γ). The slow critical manifold is expressed as $f(y) = -c\,y\,|a + b\,c\,y| + d$ with (a, b, c, d) as parameters. If we set $f(y) = a(y - y^3) + b$, where (a, b) are parameters, the system becomes the classical FitzHugh–Nagumo (FHN) model, which has origins in mid-twentieth-century biophysical modelling of the squid nerve axon[70,71]. The two different systems are illustrated in Extended Data Fig. 4. The parameters used in the comparison are $a = 1.0$, $b = 0.5$ for the classic FHN model and $a = 3.0$, $b = -3.0$, $c = 0.42$, $d = 0.9$ for the Stommel-like model. The two slow manifolds can be aligned by adding a linear transformation to equation (2), with $y \to y - y_0$, where $y_0 = -1.85$. Both the 'Stommel-like' system and the FHN system have a double-fold bifurcation, as illustrated in Fig. 3 and Extended Data Fig. 4. The system of equations used to produce Fig. 2 follows a governing set of non-dimensional equations:

$$\begin{aligned} \frac{d\Delta b}{dt} &= -(B - B_0(\gamma)) - |q_0 + q_1(\Delta b - b_0)|(\Delta b - b_0) \\ \frac{dB}{dt} &= \frac{1}{\tau}(\Delta b - \gamma) \end{aligned} \tag{3}$$

Including a Wiener process (W) with the parameter ($\sigma_{\Delta b} = \sigma_B = \sigma$) we can express equation (3) as a stochastic ordinary differential equation:

$$\begin{aligned} d\Delta b &= [-(B - B_0(\gamma)) - |q_0 + q_1(\Delta b - b_0)|(\Delta b - b_0)]dt + \sigma dW_t \\ dB &= (\Delta b - \gamma)dt/\tau + \sigma dW_t \end{aligned} \tag{4}$$

The equation for the buoyancy gradient (Δb, in $m\,s^{-2}$) (the meridional difference in buoyancy between the Southern Atlantic and Northern Atlantic) is related to the density gradient ($\Delta\rho$) through

$$\Delta b = \frac{-g}{\rho_0}\Delta\rho \tag{5}$$

using the force of gravity (g) and the mean background density (ρ_0). A linear relationship is diagnosed from the comprehensive climate model for both the

dependence of the AMOC on the meridional buoyancy gradient (Δb) and the freshwater transport ($q = q_0 + q_1 \Delta b$), which gives a measure of the salt advection feedback in the system. The buoyancy flux (B, in $m^{-2} s^{-3}$) represents the fluxes of heat and freshwater at the surface of the Southern Ocean and the North Atlantic region north of the Southern Ocean, which approximately balance on the millennial timescale (Supplementary Information). The $B_0(\gamma)$ term in equation (3) is introduced to produce horizontal shifts in the slow manifold (that is, the AABW magnitude), a property that is observed in the comprehensive model at different levels of CO_2. Given that this does not impact the position of the system fixed point on the slow manifold, the period of the D–O oscillation or the relative stadial–interstadial duration is not modified by the introduction of this parameter. The introduction of the b_0 term is used to produce vertical shifts in the slow manifold so as to span the range of physical values of the meridional buoyancy (density) gradient in the comprehensive model. The CO_2 control parameter (γ) in equations (3) and (4) is formulated in terms of buoyancy and its modifications of B_0 is parameterized as

$$B_0(\gamma) = \bar{B} + \eta(\bar{\gamma} - \gamma) \tag{6}$$

The buoyancy flux correction (equation (6)) is made up of $\bar{\gamma}$, which is a buoyancy flux at a CO_2 level in the middle of the unstable manifold, and $\bar{B}$, which is the position of the upper saddle node in non-dimensional buoyancy flux units. γ is the CO_2 level expressed in non-dimensional buoyancy units. η is chosen based on the shift in mean AABW strength as a function of CO_2 level observed in the comprehensive model. The non-dimensional system is transformed to the AABW/AMOC slow–fast system via two transformations. The meridional buoyancy gradient is used to transform from non-dimensional buoyancy to AMOC units (Sv) using the linear relation

$$\psi_{\mathrm{AMOC}} = \psi_0 + \psi_1 \Delta b \tag{7}$$

The AABW is also calculated in a similar fashion as equation (7) (Supplementary Information).

CO_2 impacts on the comprehensive model climate. When CO_2 is high (γ large) the system spends more time in the upper warm branch of the slow manifold. Warmer temperatures over the North Atlantic and Arctic reduce the mean sea-ice volume and also warm northern waters, so it takes more time for the glacial climate to terminate the AMOC. The reduced AMOC state during a D–O stadial period results in less transport of salty waters to the high northern latitudes of the North Atlantic. There is therefore a build-up of salty warm water in the low-latitude Atlantic, as has been observed in a number of modelling studies[3,25,26]. The difference observed here is that the high-CO_2 experiments have increased low-latitude Atlantic salinity built up in the upper ocean during the stadial relative to the ensemble mean (Extended Data Fig. 5), which increases the tendency to re-invigorate the AMOC, so the system spends less time in the stadial period. The converse is true at lower CO_2 levels where the system spends more time in the lower cold branch of the slow manifold. At higher CO_2 levels the temperature of the global ocean thermocline is generally larger (Extended Data Fig. 6). The Arctic and Atlantic Ocean warm more than other parts of the ocean at higher CO_2 levels. This affects the amount of heat transported to the high-latitude North Atlantic. This also impacts sea-ice growth as well as the amount of available convective potential energy for destabilization of the stadial climate state (Extended Data Fig. 6). Higher mean levels of Arctic and North Atlantic sea-ice volume are also shown to increase with decreasing atmospheric CO_2 concentration (Extended Data Fig. 7).

Data availability

Decadal average time series data from the CCSM4 model simulations are available from the University of Copenhagen Electronic Research Data Archive (ERDA): https://sid.erda.dk/cgi-sid/ls.py?share_id=Fo2F7YWBmv. All other data are provided in the Supplementary Information.

Code availability

The head code repository for this manuscript is available on Github/Zenodo: https://doi.org/10.5281/zenodo.6372628. The simple model code (https://doi.org/10.5281/zenodo.6205127) can be viewed and run online at the following mybinder.org address: https://mybinder.org/v2/gh/guidov/scdom/main?filepath=index.ipynb.

References

53. Gettelman, A. & Kay, J. E. The evolution of climate sensitivity and climate feedbacks in the community atmosphere model. *J. Clim.* **25**, 1453–1469 (2012).
54. Danabasoglu, G. et al. The CCSM4 ocean component. *J. Clim.* **25**, 1361–1389 (2012).
55. Lawrence, D. M. et al. The CCSM4 land simulation, 1850–2005: assessment of surface climate and new capabilities. *J. Clim.* **25**, 2240–2260 (2012).
56. Jahn, A. et al. Late-twentieth-century simulation of Arctic sea ice and ocean properties in the CCSM4. *J. Clim.* **25**, 1431–1452 (2012).
57. Argus, D. F., Peltier, W. R., Drummond, R. & Moore, A. W. The Antarctica component of post-glacial rebound model ICE-6G_C (VM5a) based on GPS positioning, exposure age dating of thicknesses, and relative sea level histories. *Geophys. J. Int.* **198**, 537–563 (2014).
58. Peltier, W. R., Argus, D. F. & Drummond, R. Space geodesy constrains ice age terminal deglaciation: the global ICE-6G_C (VM5a) model: global glacial isostatic adjustment. *J. Geophys. Res.* **120**, 450–487 (2015).
59. Pico, T., Birch, L., Weisenberg, J. & Mitrovica, J. Refining the Laurentide Ice Sheet at Marine Isotope Stage 3: a data-based approach combining glacial isostatic simulations with a dynamic ice model. *Quat. Sci. Rev.* **195**, 171–179 (2018).
60. Dalton, A. S. et al. Was the Laurentide Ice Sheet significantly reduced during Marine Isotope Stage 3? *Geology* **47**, 111–114 (2019).
61. Andres, H. J. & Tarasov, L. Towards understanding potential atmospheric contributions to abrupt climate changes: characterizing changes to the North Atlantic eddy-driven jet over the last deglaciation. *Clim. Past* **15**, 1621–1646 (2019).
62. Vettoretti, G. & Peltier, W. R. Last glacial maximum ice sheet impacts on North Atlantic climate variability: the importance of the sea ice lid. *Geo. Phys. Res. Lett.* **40**, 6378–6383 (2013).
63. Bryan, K. & Lewis, L. J. A water mass model of the world ocean. *J. Geophys. Res.* **84**, 2503–2517 (1979).
64. Manabe, S. & Stouffer, R. J. Two stable equilibria of a coupled ocean-atmosphere model. *J. Clim.* **1**, 841–866 (1988).
65. Jayne, S. R. The impact of abyssal mixing parameterizations in an ocean general circulation model. *J. Phys. Ocean.* **39**, 1756–1775 (2009).
66. Danabasoglu, G., Large, W. G. & Briegleb, B. P. Climate impacts of parameterized Nordic Sea overflows. *J. Geophys. Res.* **115**, C11005 (2010).
67. Shields, C. A. et al. The low-resolution CCSM4. *J. Clim.* **25**, 3993–4014 (2012).
68. Orsi, A., Johnson, G. & Bullister, J. Circulation, mixing, and production of Antarctic bottom water. *Prog. Ocean.* **43**, 55–109 (1999).
69. Wolfe, C. L. & Cessi, P. Multiple regimes and low-frequency variability in the quasi-adiabatic overturning circulation. *J. Phys. Ocean.* **45**, 1690–1708 (2015).
70. FitzHugh, R. Mathematical models of threshold phenomena in the nerve membrane. *Bull. Math. Biophys.* **17**, 257–278 (1955).
71. Nagumo, J., Arimoto, S. & Yoshizawa, S. An active pulse transmission line simulating nerve axon. *Proc. IRE* **50**, 2061–2070 (1962).

Acknowledgements

This work is a result of the ChronoClimate project, funded by the Carlsberg Foundation, and the Tipping Points in the Earth System (TiPES) project, which received funding from the European Union's Horizon 2020 research and innovation programme under grant agreement no. 820970 (G.V.). S.O.R. received support from the Villum Investigator Project IceFlow (grant no. 16572). The computations were performed at the Danish Center for Climate Computing (DC3), and we thank its administrator, R. Nuterman, for support. This is TiPES contribution no. 90.

Author contributions

G.V. conceived the study. G.V. designed and conducted the comprehensive glacial climate model simulations and developed the simple model. All authors contributed to the analysis. G.V. wrote the manuscript with contributions from all co-authors.

Competing interests

The authors declare no competing interests.

Additional information

Extended data is available for this paper at https://doi.org/10.1038/s41561-022-00920-7.

Supplementary information The online version contains supplementary material available at https://doi.org/10.1038/s41561-022-00920-7.

Correspondence and requests for materials should be addressed to Guido Vettoretti.

Peer review information *Nature Geoscience* thanks Heather Andres, Andreas Born and the other, anonymous, reviewer(s) for their contribution to the peer review of this work. Primary Handling Editor(s): James Super, in collaboration with the *Nature Geoscience* team.

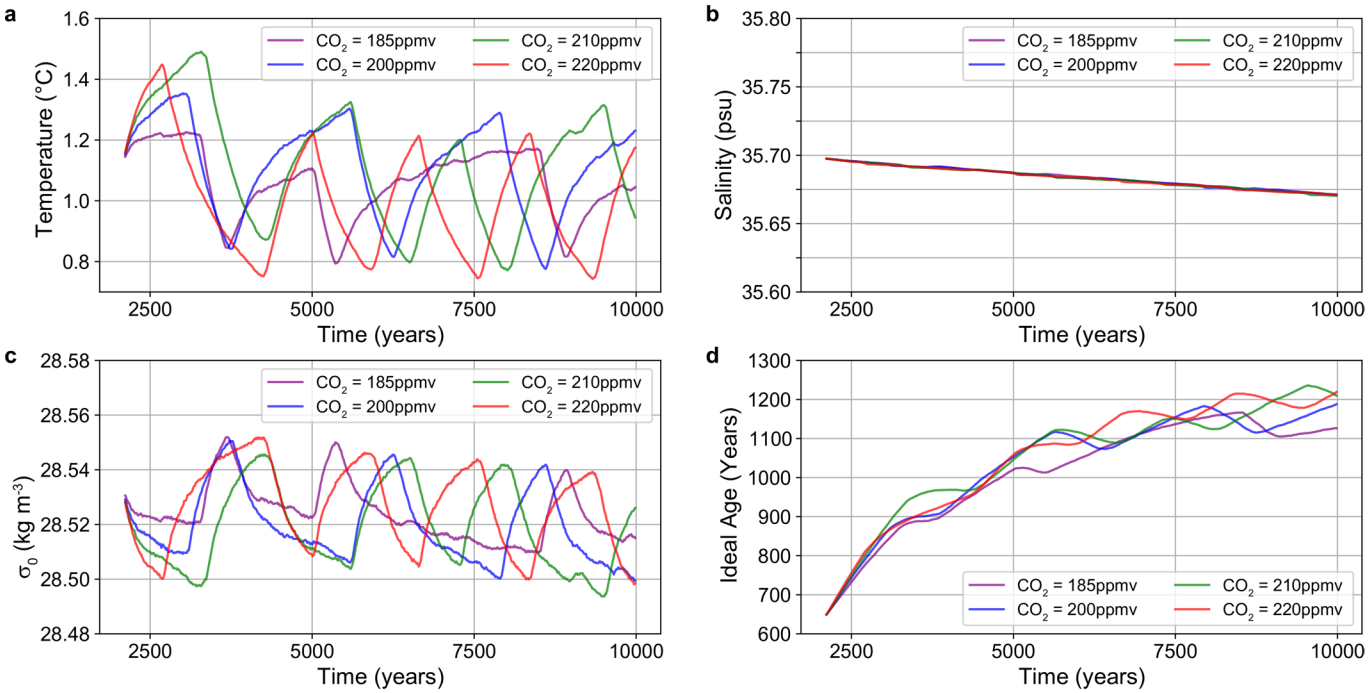

Extended Data Fig. 1 | Glacial model spinup to equilibrium. a) Timeseries of global average ocean potential temperature (°C) in four of the glacial CO_2 experiments. b) Same as for temperature but for timeseries of salinity (practical salinity units), c) potential density anomaly (σ_0: kg m^{-3}) and d) ideal age (years).

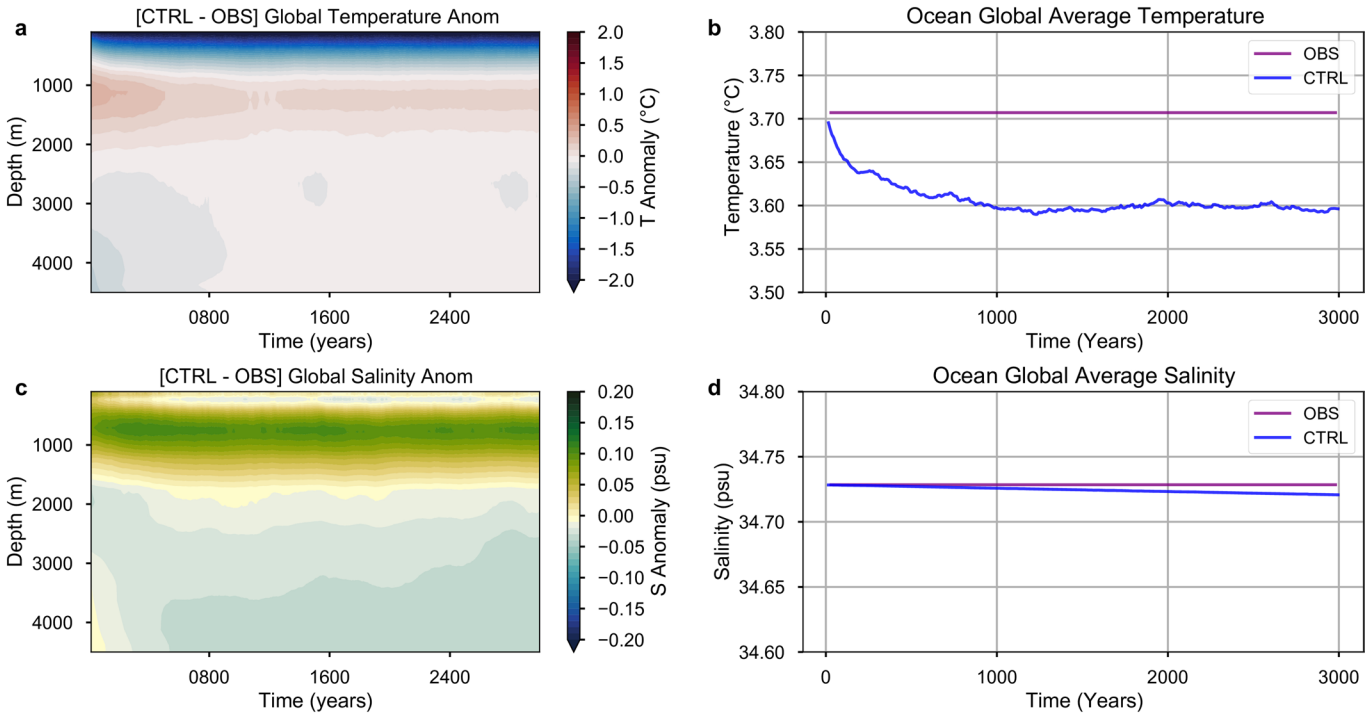

Extended Data Fig. 2 | Pre-Industrial control model validation. a) Modern global average time-depth profile of ocean potential temperature differenced from observed (°C) (see[67] for observed data). b) Global average ocean potential temperature from the modern simulation. The modern observed value is also shown in purple c) Same as in a) but for salinity (practical salinity units). Global ocean overflow parameterizations[66] have been turned off in the modern control simulation and a BL profile[63] has been used for the vertical mixing.

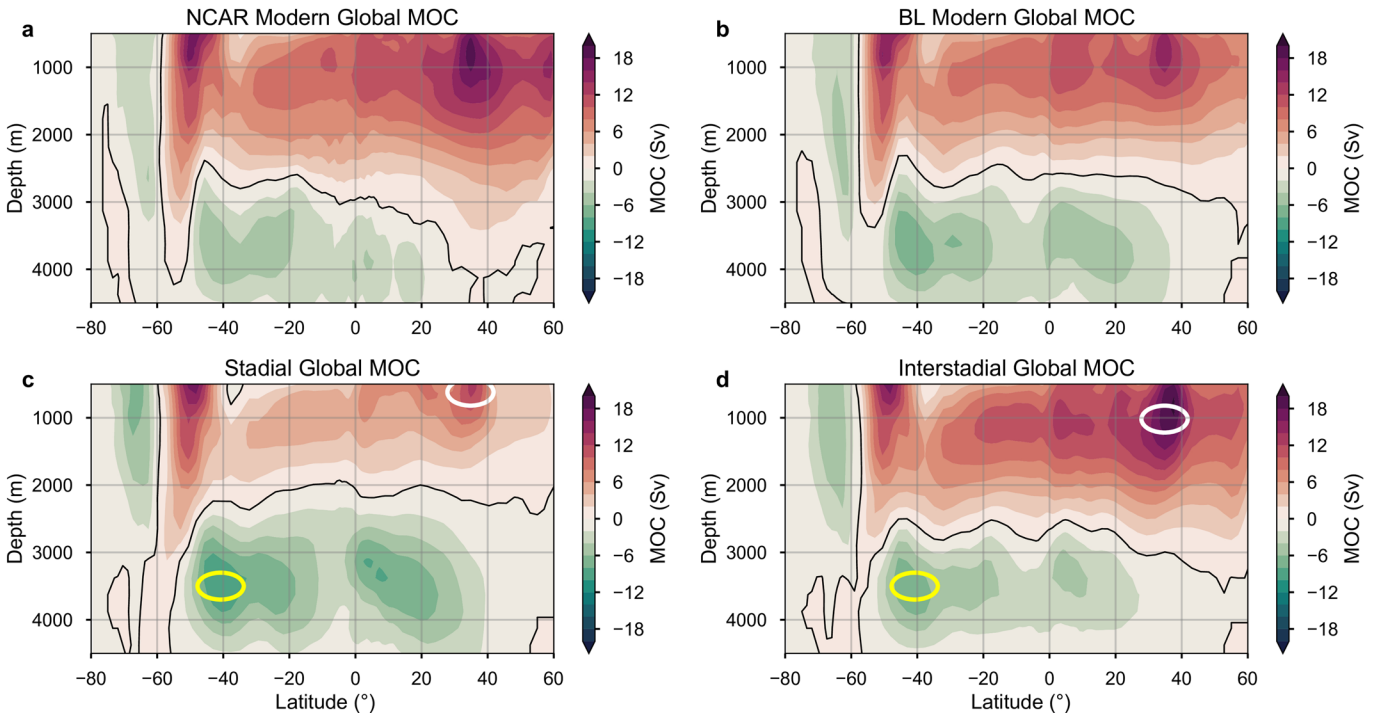

Extended Data Fig. 3 | Modern and Glacial ocean meridional overturning circulation. a) Global zonal average overturning streamfunction (Sv) from the original NCAR CCSM4 simulation described in[67]. b) Global zonal average overturning streamfunction (Sv) from the modified CCSM4 pre-industrial control simulation (BL) used in this study. The same as in b) but for the glacial c) stadial and d) interstadial climate from a simulation with CO_2=210 ppm. The maximum in NADW and AABW overturning streamfunctions (Sv) in the glacial climate are highlighted with white and yellow ellipses, respectively. These two points form the basis for the two degrees of freedom in our simple model.

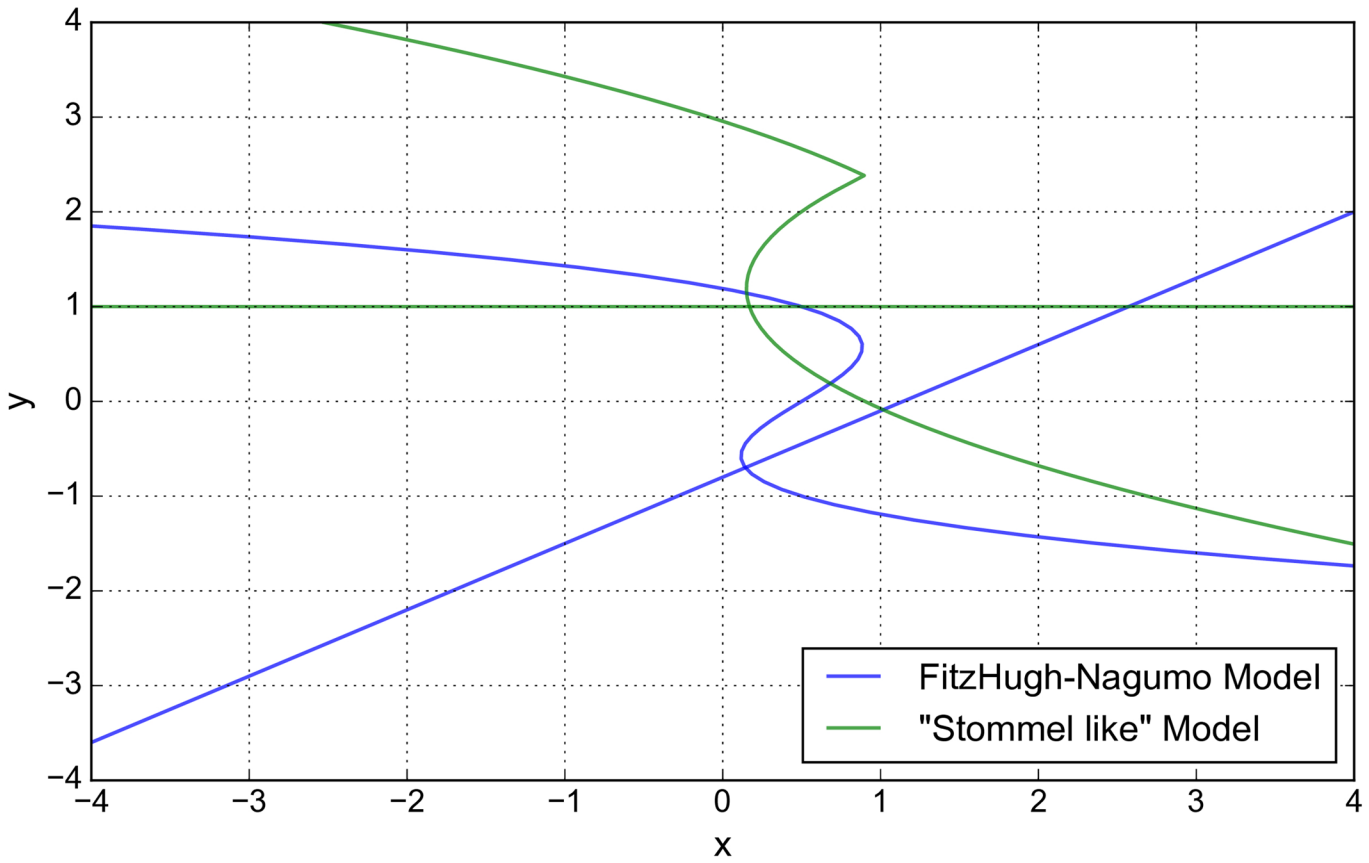

Extended Data Fig. 4 | Dynamical systems. A comparison between the Stommel-like model (green) and the FitzHugh-Nagumo model (blue)[70,71].

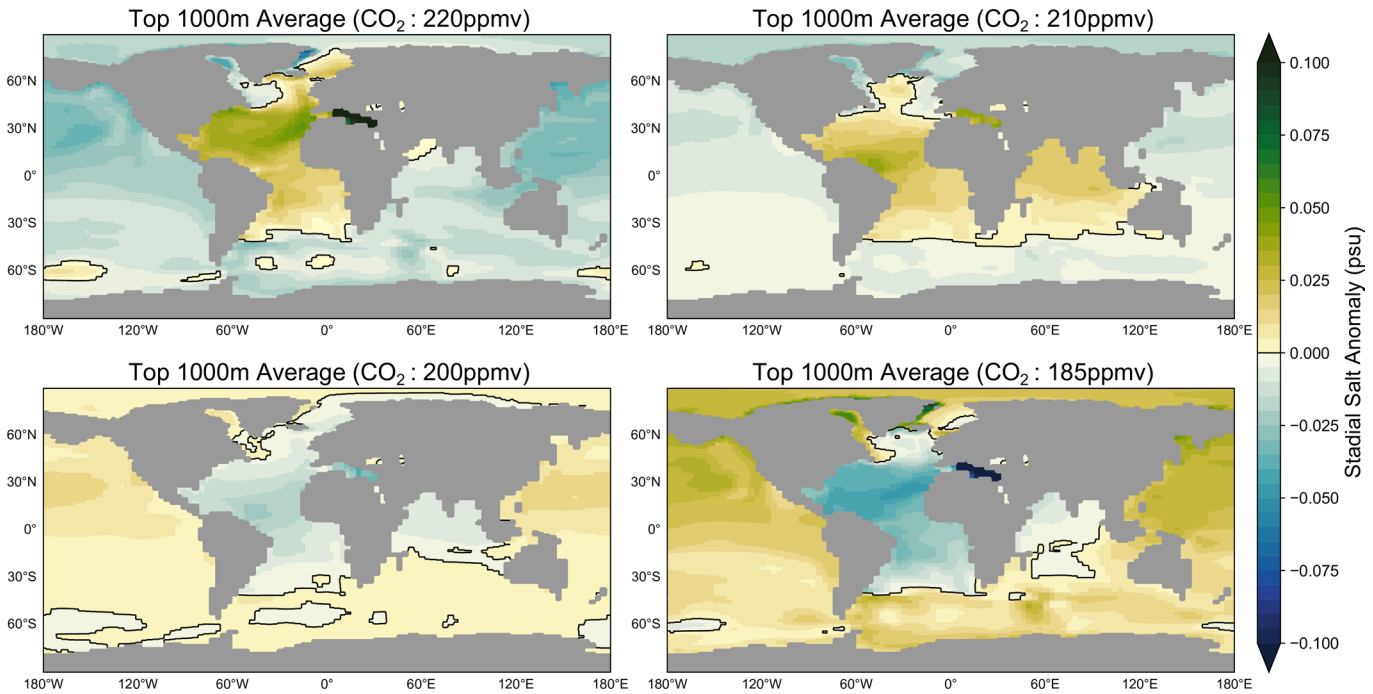

Extended Data Fig. 5 | Global thermocline salinity anomalies. The stadial salinity anomaly of each the experiments with different levels of CO_2 differenced from the ensemble mean of the four experiments. The average salinity in the top 1000 meters of the ocean in each experiment is averaged and then differenced from the ensemble mean average salinity in the top 1000 meters.

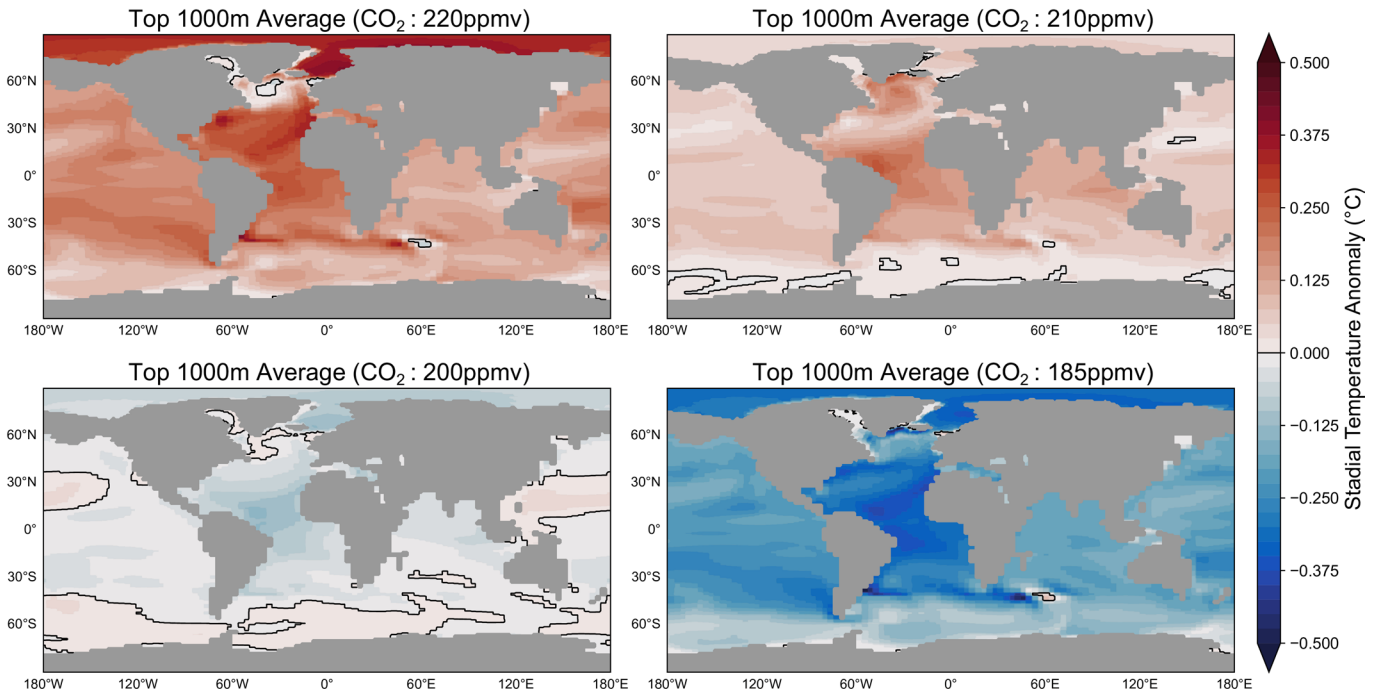

Extended Data Fig. 6 | Global thermocline temperature anomalies. The stadial temperature anomaly of each the experiments with different levels of CO_2 differenced from the ensemble mean of the four experiments. The average temperature in the top 1000 meters of the ocean in each experiment is averaged and then differenced from the ensemble mean average temperature in the top 1000 meters.

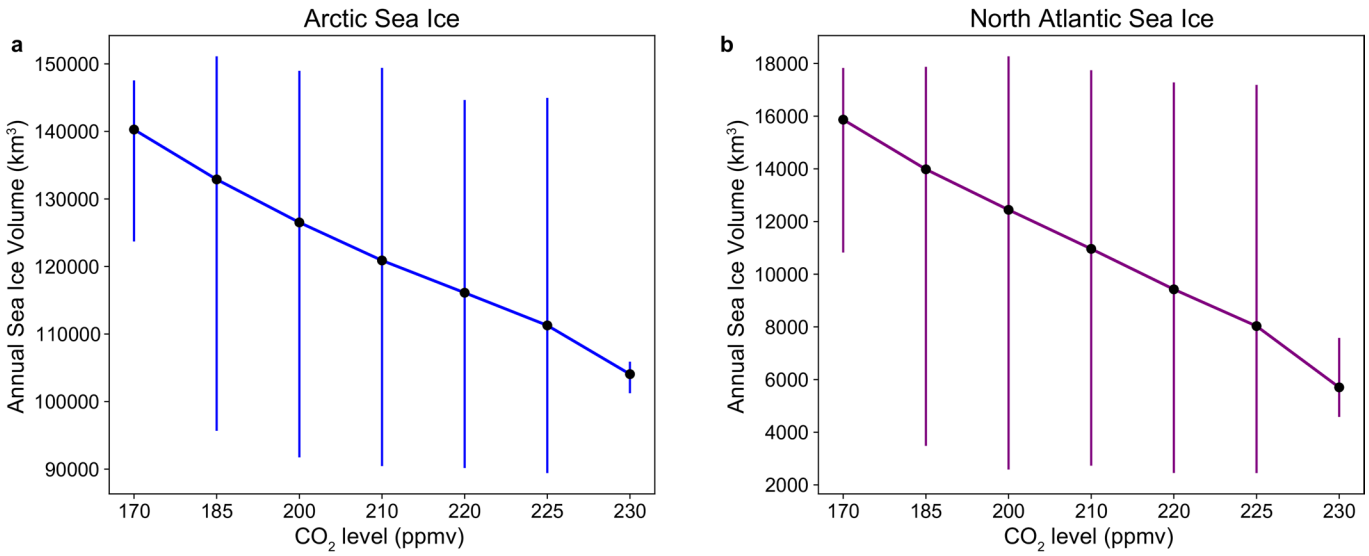

Extended Data Fig. 7 | Arctic and North Atlantic sea ice volume. Sea-ice-volume variations in the a) Arctic box and the b) North Atlantic box (see Supplementary Materials for box areas) for each of the different CO_2 simulations. The vertical lines span the range between minimum and maximum sea-ice volume for each simulation. The black dots represent the mean volume of sea-ice throughout the whole simulation. The sea-ice volume follows the characteristic pattern of a system with a fold bifurcation and a control parameter (the atmospheric CO_2 concentration).

Extended Data Table 1 | CCSM4 model simulations

Simulation	Boundary Conditions	CO_2 (ppm)	Ocean Mixing	Simulation Time (years)
1	Pre-Industrial	287	J09	3000 years
2	Pre-Industrial	287	BL79	3000 years
3	Glacial	170	BL79	8000 years
4	Glacial	185	BL79	10000 years
5	Glacial	200	BL79	8000 years
6	Glacial	210	BL79	8000 years
7	Glacial	220	BL79	8000 years
8	Glacial	225	BL79	8000 years
9	Glacial	230	BL79	10000+ years
10	Glacial	240	BL79	10000+ years
11	Heinrich	210	BL79	8000 years

List of CCSM4 experiments. Pre-Industrial Climate, Glacial Climate, and Heinrich = Glacial climate with stadial Heinrich event, CO_2 = atmospheric carbon dioxide concentration in parts per million (ppm). The tidal mixing parameterization (J09) is from[65] and the mixing profile (BL79) is from[63].